南京航空航天大学

论文集

（二〇〇九年） 第46册

高新院

南京航空航天大学科技部编

二〇一〇年五月

高 新 院

高新技术研究院2009年发表论文清单

序号	姓名	职称	单位	论文题目	刊物、会议名称	年、卷、期	类别
1	戴意涛 郭万林	博士 正高	高新院 高新院	Electric-field-induced deformation in boron nitride nanotubes	J. Phys. D: Appl. Phys.	2009.42.	
2	姜燕 郭万林	博士 正高	高新院 高新院	Temperature dependence of the stability of written bits in a magnetic hard-disk medium investigated by magnetic force microscopy	Journal of Magnetism and Magnetic Materials	2009.321.	
3	陆鹏 姜燕 郭万林	博士 正高	高新院 高新院	Electronic and magnetic properties of zigzag edge graphene nanoribbons with Stone–Wales defects	Physics Letters A	2009.373.	
4	沈荣 郭万林	博士 正高	高新院 高新院	Ion binding properties and structure stability of the NaK channel	Biochimica et Biophysica Acta	2009.1788	
5	孙晋美 郭万林	博士 正高	高新院 高新院	贝壳珍珠母多级结构的化学-力学稳定性	中国科学	2009.39.11	
6	咸小刚 郭万林	硕士 正高	高新院 高新院	厚度依赖的二氧化钛薄膜光学性能研究	纳米科技	2009.6.3	
7	张助华 郭万林	博士 正高	高新院 高新院	Electronic properties of zigzag graphene nanoribbons on Si,,001	Appl. Phys. Lett.	2009.7	
8	张助华 郭万林	博士 正高	高新院 高新院	Tunable Ferromagnetic Spin Ordering in Boron Nitride Nanotubes with Topological Fluorine Adsorption	J. AM. CHEM. SOC.	2009.131.	
9	张助华 郭万林	博士 正高	高新院 高新院	Stability and electronic properties of small boron nitride nanotubes	Journal of Applied Physics	2009.105.	
10	张助华 郭万林	博士 正高	高新院 高新院	Magnetoelectric Effect in Graphene Nanoribbons on Substrates via Electric Bias Control of Exchange Splitting	PHYSICAL REVIEW LETTERS	2009.103.	

11	张子越 郭万林	博士 正高	高新院 高新院	Stability and Electronic Properties of a Novel C-BN Heteronanotube from First-Principles Calculations	J. Phys. Chem. C	2009.113	
12	唐淳 郭万林	博士 正高	高新院 高新院	Repaly to "Mechanism for superelongation of carbon nanotubes at high temperatures"	Physical Review Letters	2009.103	
13	唐淳 郭万林	博士 正高	高新院 高新院	Molecular dynamics simulation of tensile elongation of carbon nanotubes: Temperature and size effects	Physical Review B	2009.79	
14	赵军华 郭万林	博士 正高	高新院 高新院	Elasticity of Single-Crystal Calcite by First-Principles Calculations	Journal of Computational and Theoretical Nanoscience	2009.6.	
15	钟文宇 郭万林	博士 正高	高新院 高新院	Mixed modes in opening of KcsA potassium channel from a targeted molecular dynamics simulation	Biochemical and Biophysical Research Communications	2009.388.	
16	钟文宇 郭万林	博士 正高	高新院 高新院	Kv1. 2 钾通道闭合的靶向分子动力学模拟	计算力学学报	2009.26.	
17	钟文宇 郭万林	博士 正高	高新院 高新院	KcsA 钾通道的多级开放过程:靶向分子动力学模拟	计算力学学报	2009.26.	
18	周斌 郭万林	博士 正高	高新院 高新院	Surface Concavity-Convexity Sensitive Oxidation Dynamics of Carbon Nanotubes	J. Phys. Chem. C	2009.113	
19	马燕芳 刘心声	硕士 正高	高新院 高新院	一类总体有限的随机进化博弈的极限动态	南京大学数学半年刊	2009 . 26.1	
20	周兴才 刘心声	硕士 正高	高新院 高新院	The Monte Carlo EM method for estimating multivariate tobit latent variable models	Journal of Statistical Computation and Simulation	2009 .9 .	
21	马燕芳 刘心声	硕士 正高	高新院 高新院	The Replicator Equation for a New	2008 年国际一般系统论研究会中国分会概率统	2008.	

	程龙生	正高	外校	Mechanism of Games on Graphs	计系统专业理事会（IIGSS-CB PSS）成立大会暨首届学术讨论会		
22	郭宇锋 郭万林	正高 正高	高新院 高新院	Bias voltage induced *n*- to *p*-type transition in epitaxial bilayer graphene on SiC	**Physical Review B**	2009.80	
23	戴振东 Gorb stanislav	正高 教授	高新院 国外	Contact mechanics of pad of grasshopper (Insecta: ORTHOPTERA) by finite element methods	Chinese Science Bulletin	2009.54.4.	
24	戴振东 薛群基	正高 院士	高新院	摩擦磨损的热力学研究：现状和展望	中国科学 E 辑：技术科学	2009.39.7.	
25	戴振东 薛群基	正高 院士	高新院	Progress and deuelopment in thermodynamic theory of friction and wear	Science in china series E	2009.52.4.	
26	杨志贤 戴振东	博士 正高	高新院 高新院	东方龙虱鞘翅：形态学及力学性能研究	科学通报	2009.54.12.	
27	王周义 王金童 吉爱红 戴振东	博士 硕士 副高 正高	高新院	虎纹捕鸟蛛运动反力测试	自然科学进展	2009.19.8.	
28	杨志贤 戴振东 王卫英	博士 正高 副高	高新院 高新院 机电	东方龙虱（雄性）抱握足形态学及吸附特性	复合材料学报	2009.26.3.	
29	程湛 戴振东	硕士 正高	高新院 高新院	基于 HSV 空间的大壁虎脑图谱图像分割研究	现代电子技术	2009.4. 总 291.	
30	李宏凯 戴振东 石爱菊 张昊	博士 正高 副高 中级	高新院 高新院 外校 高新院	Angular observation of joints of geckos moving on horizontal and vertical surfaces	科学通报(英文版)	2009.29.5.	
31	管兴伟 张昊 吉爱红 戴振东	硕士 中级 副高 正高	高新院	爬壁机器人尖爪型仿生脚掌设计	机电工程	2009.26.2.	
32	戴振东	正高	高新院	Redundancy closured frictional force generated among toes of gecko	World Tribology Congress World Tribology Congress 2009	2009	
33	戴振东	正高	高新院	Biomimetics of gecko locomotion: from biology to engineering	Reconfigurable mechanisms and robots 2009	2009	
34	李宏凯 樊鸣鸣	博士 硕士	高新院 高新院	便携式人体皮肤摩擦性能测试仪的研制	摩擦学学报	2009.29.6.	

	弓娟琴 戴振东	正高 正高	外校 高新院				
35	郭东杰 丁海涛 韦海菊 何青松 于敏 戴振东	副高 硕士 硕士 硕士 副高 正高	高新院	Hybrids perfluorosulfonic acid ionomer and silicon oxide membrane for application in ion-exchange polymer-metal composite actuators	SCIENCE IN CHINA SERIES E-TECHNOLOGICAL SCIENCES	2009.52.10	
36	郭东杰 王晶 谭伟 肖守军 戴振东	副高 硕士 正高 正高 正高	高新院 高新院 高新院	Macroporous silicon templated from silicon nanocrystallite and functionalized Si-H reactive group for grafting organic monolayer	JOURNAL OF COLLOID AND INTERFACE SCIENCE	2009.52.10	
37	郭策 蔡雷 谢合瑞 王周义 戴振东 孙久荣	正高 博士 硕士 博士 正高 正高	高新院 高新院 高新院 高新院 高新院 北大	The divisional and hierarchical innervations of G. gecko's toes to motion and reception	Chinese Science Bulletin	2009.54.16	
38	谢合瑞 郭策 戴振东	硕士 正高 正高	高新院	恒流多通道动物机器人遥控刺激系统的研制	现代电子技术	2009.4	
39	郭策 蔡雷 谢合瑞 王周义 戴振东 孙久荣	正高 博士 硕士 博士 正高 正高	高新院	大壁虎脚趾运动和感觉的分区分级调控	科学通报	2009.54.7	
40	刘彬 张昊 郭东杰 戴振东	硕士 中级 副高 正高	高新院	倾斜仿生刚毛的设计、制备及黏附性能研究	摩擦学报	2009.29.5	
41	张昊 成佳伟 肖世旭 戴振东	中级 硕士 硕士 教授	高新院	大壁虎运动体态及其步态相关性的实验研究	自然科学进展	2009.12	
42	王文波 郭策 孙久荣 戴振东	中级 正高 正高 正高	高新院	Locomotion Elicited by Electrical Stimulation in the Midbrain of the Lizard Gekko gecko	Intelligent Unmanned Systems: Theory and Applications	2009.192	
43	黄护林 周小明	正高 博士	高新院	The impacts of normal magnetic field on the	ASME Journal of Heat Transfer	2009.4	

				instability of thermocapillary convection in a two-layer fluid system			
44	黄护林 李博	正高 硕士	高新院	Heat Transfer of Free Surface MHD-Flow with a Wall of Non-uniform Electrical Conductivity	23rd IEEE Symposium on Fusion Engineering 2009	2009.6	
45	周小明 黄护林	博士 正高	高新院	MHD effect on the development of thermocapillary convection in a two-layer fluid system	International Journal of Low-Carbon Technologies	2009.9	
46	周小明 黄护林	博士 正高	高新院	MHD effect on interfacial deformation of thermocapillary convection in two-Layer system	Microgravity Science and Technology	2009.10	
47	周小明 黄护林	博士 正高	高新院	基于 level set 方法的双层流体热毛细对流数值研究	2009 年中国工程热物理学会传热传质分会	2009.11	
48	李博 黄护林	硕士 正高	高新院	Heat Transfer Enhancement of Free Surface MHD-Flow by a Dimpled Wall	Journal of Enhanced Heat Transfer	2009.10	
49	李博 黄护林	硕士 正高	高新院	球凸板对磁场中导电流体自由表面流动的传热强化	化工学报	2009.7	
50	黄富来 黄护林	博士 正高	高新院	磁场对高超声速弱电离气体流动的影响	航空学报	2009.10	
51	黄富来 黄护林	博士 正高	高新院	高超声速化学非平衡流动 MHD 效应的数值模拟	工程热物理学报	2009.11	
52	黄富来 黄护林	博士 正高	高新院	均匀磁场中高超声速弱电离气体流动数值模拟	航空动力学报	2009.11	
53	蔡亮 黄护林	博士 正高	高新院	轴向磁场作用下绕流圆柱的稳定性研究	2009 年中国工程热物理学会传热传质分会	2009.11	
54	高益兵 黄护林	硕士 正高	高新院	一种新型碟式聚光镜的设计与模拟	2009 年中国工程热物理学会传热传质分会	2009.11	
55	曹鑫暐 黄护林	硕士 正高	高新院	方腔内 Rayleigh-Bernard 对流温度场的三维重建	2009 年江苏省工程热物理学会传热传质分会	2009.11	

56	周飞 袁英光 王晓雷 王美玲	正高 硕士 正高 副高	高新院 051 材料院 051	Influence of nitrogen ion implantation fluences on surface structure and tribological properties of SiC ceramics in water-lubrication	Applied Surface Science	2009.255.9	
57	周飞 袁英光 陈康敏 王晓雷	正高 硕士 副高 正高	高新院 051 外校 材料院	Influence of nitrogen ion implantation energies on surface chemical bonding structure and mechanical properties of nitrogen-implanted silicon carbide ceramics	Nuclear Instruments and Methods in Physics Research B	2009.267.17	
58	周飞 王远 刘峰 孟月东 戴振东	正高 硕士 副高 正高 正高	高新院 051 外校 外校 高新院	Friction and wear properties of duplex MAO/CrN coatings sliding against Si3N4 ceramic balls in air, water and oil	Wear	2009.267.9-10	
59	张振夫 周飞 王晓雷 陈建宁 云乃彰 李建桥	硕士 正高 副高 中级 正高 正高	高新院 高新院 051 051 051 外校	滑动表面仿生微结构的摩擦学效应	机械制造与自动化	2009.38.3	
60	王霄 周飞 潘建跃 张中元	硕士 正高 副高 中级	高新院 高新院 外单位 外单位	钛合金表面微弧氧化技术的研究进展	机械制造与自动化	2009.38.4	
61	周芳 周飞	硕士 正高	高新院 材料院	水润滑硅基非氧化陶瓷摩擦学性能及其表面改性研究进展	润滑与密封	2009.34.2	
62	周飞 岳宾 足立幸志 加藤康司	正高 硕士 副高 正高	高新院 051 国外 国外	Friction and wear properties of amorphous carbon nitride coatings sliding against Silicon carbide balls in water-ethanol and water-glycol mixtures	2nd European Conference on Tribology 2009	2009	
63	周飞 周芳 王美玲 王晓雷	正高 硕士 副高 正高	高新院 06 06 051	Friction and Wear Properties of C Ion Implanted Silicon Nitride against Silicon Nitride Balls in Water Lubrication	4th World Tribology Congress 2009	2009	

64	周飞 岳宾	正高 硕士	高新院 051	非晶氮化碳薄膜在乙醇-水溶液中的摩擦磨损特性研究	2009 全国青年摩擦学学术会	2009	
65	王宪良 周飞 张振夫 云乃彰 陈建宁 王晓雷	硕士 正高 硕士 正高 副高 正高	机电 高新院 051 052 052 051	钛合金表面微结构在水润滑中摩擦特性研究	2009 全国青年摩擦学学术会	2009	
66	孔志强 周飞 王美玲 吴雪梅	硕士 正高 副高 正高	材料院 高新院 材料院 外校	稀土 Ho2O3 掺杂对 ZnO :CaO 陶瓷介电性能影响	功能材料	2009.40.增刊	
67	杨宇晓 刘海颖	初级 中级	高新院 高新院	用于信号波达方向估计的共轭 ESPRIT 算法及性能分析	电讯技术	2009.49.12	
68	刘海颖 王惠南 陈志明 叶伟松	中级 正高 博士 中级	高新院 航天院 高新院 高新院	喷气/偏置动量轮联合微小卫星三轴稳定控制	系统仿真学报	2009.21.7	
69	刘海颖 杨宇晓 王惠南	中级 初级 教授	高新院 高新院 航天院	卫星编队飞行的光通信研究	遥测遥控	2009.30.5	
70	庄丽葵 丁萌 曹云峰	中级 博士 教授	高新院 三院 高新院	一种地平线语跑道边缘线检测方法	传感器与微系统	2009.28.12	
71	何火军 曹云峰 刘兴华	硕士 教授 博士	高新院 高新院 三院	无人机飞行控制系统虚拟样机平台	应用科学学报	2009.27.6.	
72	丁萌 曹云峰 吴庆宪	博士 教授 教授	三院 高新院 校机关	月面灰度图像中的陨石坑检测	应用科学学报	2009.27.2.	
73	丁萌 曹云峰 吴庆宪	博士 教授 教授	三院 高新院 校机关	基于 Census 变换和 Boosting 方法的陨石坑区域检测	南京航空航天大学学报	2009.41.5.	
74	蔡晟 曹云峰	硕士 教授	三院 高新院	无尾翼无人机横侧向分析与增稳控制设计	控制工程	2009.16.S2	
75	丁萌 曹云峰 吴庆宪	博士 教授 教授	三院 高新院 校机关	基于被动图像中的探测器着陆过程中岩石检测	光电工程	2009.36.1.	
76	丁萌 曹云峰 吴庆宪	博士 教授 教授	三院 高新院 校机关	月球探测器着陆中基于被动图像的着陆场收索及斜坡估计	宇航学报	2009.30.6.	

77	丁萌 曹云峰 吴庆宪	博士 教授 教授	三院 高新院 校机关	一种从月面图像检测陨石坑的方法	宇航学报	2009.30.3.	
78	丁萌 曹云峰 吴庆宪	博士 教授 教授	三院 高新院 校机关	Method of Passive Imaging Based Crater Autonomous Dhinese Journai of Aeronautics	航空学报	2009.22.3.	
79	张珍 曹云峰	硕士 教授	三院 高新院	基于数学形态和支持向量机的跑到检测方法	火力与指挥控制	2009.34.9.	
80	刘兴华 曹云峰	博士 教授	三院 高新院	模型驱动的复杂反应式系统顶层设计与验证	系统仿真学报	2009.21.14.	
81	刘中杰 曹云峰	博士 教授	三院 高新院	基于视觉的无人作战飞机着陆系统研究	红外与激光工程	2009.38.S1.	
82	李航 曹云峰	博士 教授	三院 高新院	基于视觉的无人作战飞机自主着陆系统的软件研究	红外与激光工程	2009.38.S1.	
83	陈超 曹云峰	博士 教授	三院 高新院	倾转旋翼机动态逆滑模变结构控制器设计	2009 .第三届中国导航，制导与控制学术会议上交流	会议论文集P431-434	
84	程尚 曹云峰	博士 教授	三院 高新院	倾转旋翼飞行器空气动力学模型研究	2009 .第三届中国导航，制导与控制学术会议上交流	会议论文集P431-434	
85	谢娟 曹云峰	博士 教授	三院 高新院	侦察攻击型无人机飞行器管理计算机设计	2009 .第三届中国导航，制导与控制学术会议上交流	会议论文集P431-434	
86	邹小志 曹云峰	博士 教授	三院 高新院	飞翼式微型飞行器动力学特性分析	佳木斯大学学报	2009.27.6.	

IOP PUBLISHING JOURNAL OF PHYSICS D: APPLIED PHYSICS

J. Phys. D: Appl. Phys. **42** (2009) 085403 (4pp) doi:10.1088/0022-3727/42/8/085403

Electric-field-induced deformation in boron nitride nanotubes

Yitao Dai, Wanlin Guo[1], Zhuhua Zhang, Bin Zhou and Chun Tang

Institute of Nano Science, Nanjing University of Aeronautics and Astronautics, Nanjing 210016, People's Republic of China

E-mail: wlguo@nuaa.edu.cn

Received 17 September 2008, in final form 29 January 2009
Published 26 March 2009
Online at stacks.iop.org/JPhysD/42/085403

Abstract

Axial deformation of boron nitride nanotubes (BNNTs) induced by an external electric field is studied by density functional theory. It is found that the field-induced deformation can reach 1% at a field strength of around 10 V nm^{-1} due to both the converse piezoelectric effect and the electrostrictive effect. This deformation is about nine times larger than that of traditional piezoceramics and can be enhanced with increasing length or decreasing diameter of the BNNTs. The corresponding volumetric work capacity is calculated to be two orders of magnitude higher than those of traditional piezoceramics.

(Some figures in this article are in colour only in the electronic version)

1. Introduction

Materials for converting electrical energy into mechanical energy are essential for nano-electromechanical devices [1]. Piezoelectric effects [3], electrostrictive effects [4] and flexoelectric effects [5–8] have been found for electromechanical coupling in bulk as well as nano materials. Piezoceramics are the most widely used energy conversion materials, but their typical deformation level is only about 0.1% strain with a low fracture toughness. Polymer electrostrictive materials can suffer from much higher strain levels than those of traditional piezoceramics materials but have low Young's modulus. Until recently, for most of the reported artificial energy conversion materials, the volumetric work densities are below 3.4 MJ m^{-3} [4]. It is reported that carbon nanotubes (CNTs) have giant electrostrictive deformation and can be stretched by an external electric field (E_{ext}) with strain up to 10%. Since CNTs have high Young's modulus, their volumetric work densities are calculated to be three orders higher than those of piezoceramics and polymer electrostrictive materials [4]. However, there are still some limitations for CNT-based energy conversion materials. For example, CNTs are thought to be chemically active and could be easily oxidized at a high temperature [9–13]. What is more, they are either conductors or narrow gap semiconductors [14, 15] and hence may not be suitable for the situations where insulators are required. So seeking new energy conversion materials with a high work density is of great significance.

BNNTs have Young's modulus of about 0.7 TPa, similar to those of CNTs [16, 17]. Therefore, the volumetric work densities of BNNTs for energy conversion are expected to be comparable to those of CNTs under the same strain. Moreover, BNNTs have an onset temperature for oxidation up to 800 °C, much higher than that of CNTs of only 400 °C, and thus are far more resistant to oxidation at high temperature [18, 19]. Finally, BNNTs are wide-gap semiconductors with a quasiparticle band gap of about 5.5 eV [20, 21], which makes them liable to suffer from a high breakdown voltage [22–24]. Therefore, BNNTs should be good energy conversion materials if they have large electric-field-induced deformation ($D_{induced}$).

Unfortunately, theoretical studies have predicted that boron nitride nanotubes (BNNTs) have a piezoelectricity with response values much smaller than those of ZnO and the piezoceramics materials [25]. However, it is known that zigzag BNNTs should have an electrostrictive effect except for a piezoelectric effect [26–28]. Thus, for a full understanding of the performances of BNNTs as energy conversion materials, the electrostrictive effect should not be ignored, especially when the field strength is very high. In this paper, the axial deformation of BNNTs in an external electric field is directly investigated by first-principles calculations. It is found that the longitudinal deformation can reach up to 1% when an axial electric field around 10 V nm^{-1} is applied from the B

[1] Author to whom any correspondence should be addressed.

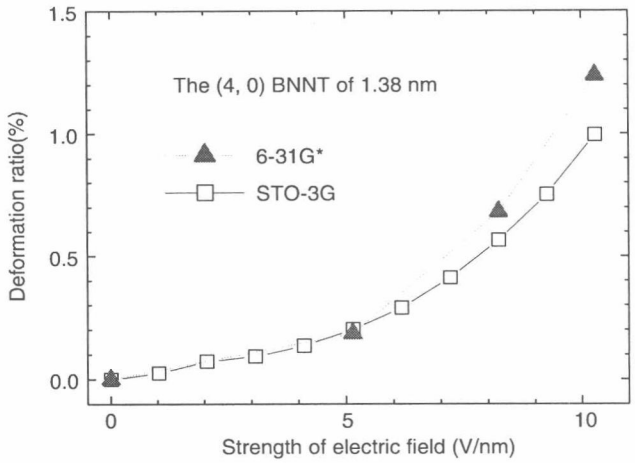

Figure 1. Electric-field-induced deformation of a 1.38 nm (4, 0) BNNT obtained by the DFT calculations using the STO-3G and 6-31G* basis sets.

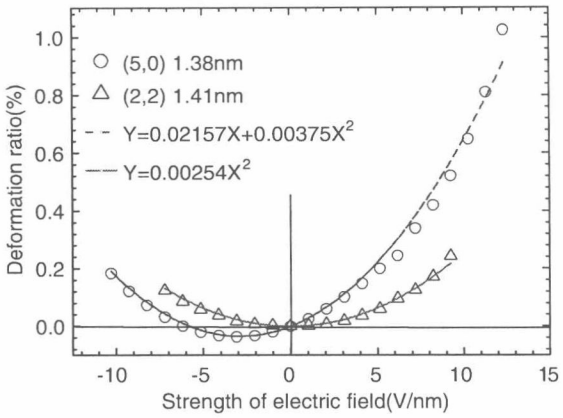

Figure 2. Axial deformation of the hydrogen-terminated open-end (5, 0) and (2, 2) BNNTs in an external electric field (E_{ext}). The electric field is applied along the tube axis. For zigzag BNNTs, the positive E_{ext} is defined from the B end to the N end in this work.

end to the N end, and it increases with increasing tube length or decreasing tube diameter, at least in the narrow range of the calculated zigzag BNNTs. The $D_{induced}$ arises from both the converse piezoelectric effect and the electrostrictive effect, and the electrostrictive deformation can be twice the piezoelectric deformation.

2. Modelling and methods

The structure optimizations are performed using density functional theory (DFT) within the linear combination of atomic orbitals (LCAO) assumption and the local density approximation (LDA). The B3LYP exchange correlation potential and the free-atom basis sets (STO-3G) [4] are used for the DFT calculations. The STO-3G basis sets may be too small for the electronic structure calculation, but it is enough for the geometry structure optimization [29]. To verify the reliability of the method we used, 6-31G* basis sets are also used for the same system as a comparison. As shown in figure 1, for a (4, 0) BNNT of 1.38 nm, the coincidence in the calculated results of field-induced deformation by the two kinds of basis sets is excellent, which demonstrates that the STO-3G basis sets work sufficiently to study the field-induced deformation of BNNTs. The relative energies are guaranteed to converge to 10^{-6} eV atom^{-1}. All the quantum mechanics calculations in this work are carried out using the PCGAMESS package [30].

3. Results and discussion

To show the deformation behaviour of armchair and zigzag BNNTs in axial electric field, a (2, 2) BNNT and a (5, 0) BNNT with similar lengths are modelled as examples. The small BNNTs are expected to be synthesized since recent calculations have shown that even the (3,0) BNNT can be stable well over room temperature [31]. The dangling bonds at the tube ends are uniformly terminated with hydrogen atoms. The initial lengths of the energy optimized (2, 2) and (5, 0) BNNTs are about 1.41 nm and 1.38 nm (the hydrogen atoms are not taken into account), respectively. E_{ext} is applied along the tube axis and the positive direction is defined from the B end to the N end for the zigzag BNNTs. Figure 2 shows the deformation ratios of the (5, 0) and (2, 2) BNNTs as functions of E_{ext}. The (5, 0) BNNT is elongated when a positive E_{ext} is applied, and the deformation ratio increases with increasing E_{ext}. When E_{ext} reaches 12.4 V nm^{-1}, strikingly, the deformation ratio is found over 1%, which is about nine times higher than that of traditional piezoceramics [4]. As the (5, 0) BNNT has a Young modulus of about 0.724 TPa when the thickness is taken as 0.34 nm [32], the corresponding volumetric work density per cycle for a matched mechanical load, which is proportional to $\frac{1}{2}Y\varepsilon_m^2$, is calculated to be 36 MJ m^{-3} (here, Y is the Young modulus of the BNNTs and ε_m is the maximum deformation ratio.). This value is only lower than that of CNTs and is at least nine times higher than those of other energy conversion materials in [4], with the highest of 3.4 MJ m^{-3}, and is over 100 times higher than those of traditional piezoceramics materials. However, when a reversed E_{ext} is applied, asymmetric deformation behaviour is found. In this case, the BNNT is compressed when E_{ext} is smaller than 3 V nm^{-1} and then it is elongated thereafter. In contrast, the situation is different for the (2, 2) BNNT; it is always elongated gradually as the field strength increases regardless of the field direction, but with a much smaller deformation ratio. A similar E_{ext}-deformation curve is also found for a (3, 3) BNNT of 1.26 nm, with only a slight difference from that of the (2, 2) BNNT.

The different behaviour between zigzag and armchair BNNTs in the electric field arises from their distinctly different structures. In zigzag BNNTs, the B and N atoms distribute along the tube axis layer by layer, giving rise to axial spontaneous polarization [25, 33]. Here the $D_{induced}$ arises from both the converse piezoelectric effect and the electrostrictive effect. But in armchair BNNTs, each layer has the same number of B or N atoms, no axial spontaneous polarization exists and thus no axial piezoelectricity can be found. These opinions are confirmed by the fact that the calculated results can be fitted very well by the curves with

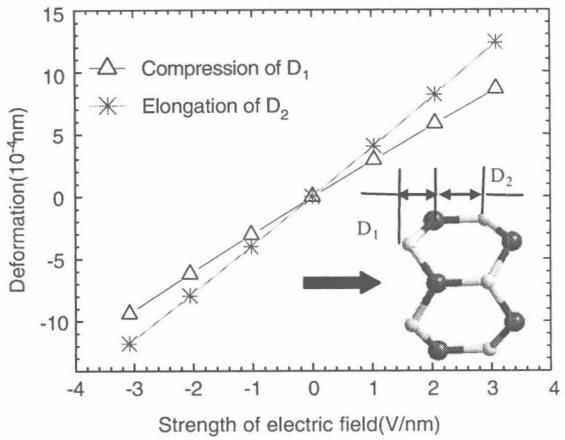

Figure 3. (Colour online) Two deformation components as functions of the electric field. The inset shows two cells in a (5, 0) BNNT. The bright (grey) and dark (blue) balls denote the B and N atoms, respectively. The positive electric field is indicated by the thick arrow, which is applied from the B end to the N end.

the expressions of $Y = 0.02157X + 0.00375X^2$ and $Y = 0.00254X^2$ for the (5, 0) and (2, 2) BNNTs, respectively. Here, the first and second order terms can be recognized as the contributions of the converse piezoelectric effect and the electrostrictive effect [26], respectively. When the electric field is 12 V nm^{-1}, the electrostrictive deformation is about twice the piezoelectric deformation.

To better understand the D_{induced} of the (5, 0) BNNT, a detailed analysis of its structure is needed. According to the atomic structure, each unit of the (5, 0) BNNT can be separated into two cells, as shown in the inset of figure 3, with the axial lengths denoted as D_1 and D_2, respectively. When a positive electric field is applied, the former cell is shortened and the latter cell is elongated. Our calculations show in detail that the elongation of D_2 is larger than the compression of D_1, giving rise to the elongation of the BNNT. In contrast, D_1 is elongated with a smaller deformation than the compression of D_2 in the reversed field, leading to overall compression of the (5, 0) tube.

To study the size effect on the D_{induced} of zigzag BNNTs, (5, 0) BNNTs with three different lengths (about 1.1 nm, 1.56 nm, 1.77 nm, respectively) and (4, 0), (6, 0), (7, 0) BNNTs with the same length of 1.38 nm are also modelled. Figure 4(*a*) shows the D_{induced} of the (5, 0) BNNTs with different lengths as functions of the field strength. It is found that the D_{induced} increases with increasing tube length at a given positive E_{ext}. This trend can be well understood by analysing the electronic properties of the BNNTs with different tube lengths. As shown in table 1, the energy gap between the highest occupied molecular orbital (HOMO) and the lowest unoccupied molecular orbital (LUMO) decreases with increasing tube length and finally leads to an increase in polarizability. Therefore, it can be expected that the longer tubes should be much more easily polarized and have a larger converse piezoelectricity constant and hence exhibit larger deformation in the same positive E_{ext}. Figure 4(*b*) shows the effect of the tube diameter on the deformation behaviour. For the BNNTs with the same length, the D_{induced} decreases

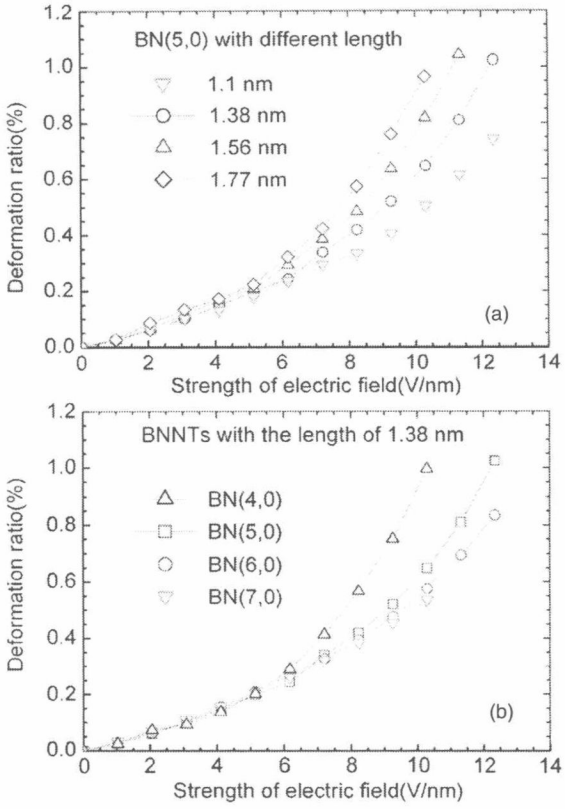

Figure 4. (*a*) Electric-field-induced deformation of the (5, 0) BNNTs with different lengths. (*b*) Electric-field-induced deformation of zigzag BNNTs with different diameters.

Table 1. Energy gaps (E_{gap}) between the HOMO and the LUMO and axial polarizabilities (P_{zz}) of (5, 0) BNNTs with different lengths. The polarizabilities are calculated using the time-dependent HF (TDHF) [34] method with the STO-3G basis sets.

Length (nm)	1.1	1.38	1.56	1.77
E_{gap} (eV)	3.36	3.21	3.07	2.93
P_{zz} (au/atom)	7.18	7.39	7.65	7.94

with increasing tube diameter at a given positive field strength. This phenomenon originates mainly for two reasons. One is similar to the reason referred to above, as shown in table 2, the energy gap increases with increasing tube diameter due to the weakened curvature effect [32], resulting in a decrease in polarizability. Another reason is that larger tubes have higher Young's modulus [32] and are more difficult to deform. The decrease in D_{induced} in larger BNNTs may hinder the applications of large BNNTs as energy conversion materials. Fortunately, both the energy gap and the Young modulus will gradually become stable with increasing tube diameter [32]. Consequently, it can be expected that with increasing diameter, tubes with the same length will have smaller D_{induced}, but the reduction in D_{induced} will become slower for larger BNNTs.

4. Conclusion

In conclusion, BNNTs, especially small and long zigzag BNNTs, are predicted to be attractive energy conversion

Table 2. E_{gap} and P_{zz} of zigzag BNNTs with different tube diameters at a length of 1.38 nm.

Tube type	(4, 0)	(5, 0)	(6, 0)	(7, 0)
E_{gap} (eV)	1.56	3.21	4.38	5.02
P_{zz} (au./atom)	7.65	7.39	7.33	7.23

materials. In the zigzag BNNTs, the electric-field-induced deformation, which arises from both the piezoelectric effect and the electrostrictive effect, can reach up to 1% in an axial electric field of around $10\,V\,nm^{-1}$, about nine times higher than those of piezoceramic materials. The corresponding volumetric work capacity is $36\,MJ\,m^{-3}$, which is only lower than that of CNTs, but nearly ten times higher than all the other reported energy conversion materials [4]. Armchair BNNTs have no piezoelectric effect but still have an electrostrictive effect. Considering the chemical inertness and electrical insulation, BNNTs should be of great value in potential applications.

Acknowledgments

This work is supported by the 973 Program (2007CB936204), the Ministry of Education (705021, IRT0534) and National and Jiangsu NSF (10732040, BK2008042) of China.

References

[1] Baughman R H *et al* 1999 *Science* **284** 1340
[2] Wang X D, Song J H, Liu J and Wang Z L 2007 *Science* **316** 102
[3] Wang Z L and Song J H 2006 *Science* **312** 242
[4] Guo W and Guo Y 2003 *Phys. Rev. Lett.* **91** 115501
[5] Tagantsev A K 1986 *Phys. Rev.* B **34** 5883
[6] Majdoub M S, Sharma P and Cagin T 2008 *Phys. Rev.* B **77** 125424
[7] Kalinin S V and Meunier V 2008 *Phys. Rev.* B **77** 033403
[8] Naumov I, Bratkovsky A M and Ranjan V 2008 arXiv:0810.1775
[9] Mirfakhrai T, Madden J D W and Baughman R H 2007 *Mater. Today* **10** 30
[10] Tang C, Guo W and Guo Y 2006 *Appl. Phys. Lett.* **88** 243112
[11] Guo W and Guo Y 2004 *Acta Mech. Sin.* **20** 192
[12] Cabria I, Amovilli C, López M J, March N H and Alonso J A 2006 *Phys. Rev.* A **74** 063201
[13] Collins P G, Bradley K, Ishigami M and Zettl A 2000 *Science* **287** 1081
[14] Chan S, Chen G, Gong X G and Liu Z 2003 *Phys. Rev. Lett.* **90** 068403
[15] Crespi V H, Cohen M L and Rubio A 1997 *Phys. Rev. Lett.* **79** 2093
[16] Postma H W Ch, Teepen T, Yao Z, Grifoni M and Dekker C 2001 *Science* **293** 76
[17] Suryavanshi A P, Yu M F, Wen J, Tang C and Bando Y 2004 *Appl. Phys. Lett.* **84** 2627
[18] Golberg D, Bando Y, Kurashima K and Sato T 2001 *Scr. Mater.* **44** 1561
[19] Chopra N G, Luyhen R J, Cheney K, Crespi V H, Cohen M, Louie S G and Zettl A 1995 *Science* **269** 966
[20] Chen Y, Stewart J Z, Campbell J and Le Caer G 2004 *Appl. Phys. Lett.* **84** 13
[21] Rubio A, Corkill J L and Cohen M L 1994 *Phys. Rev.* B **49** 5081
[22] Blasé X, Rubio A, Louie S G and Cohen M L 1994 *Europhys. Lett.* **28** 335
[23] Cumings J and Zettl A 2004 *Solid State Commun.* **129** 661
[24] Bai X, Golberg D, Bando Y, Zhi C, Tang C, Mitome M and Kurashima K 2007 *Nano Lett.* **7** 632
[25] Nakhmanson S M, Calzolari A, Meunier V, Bernholc J and Buongiorno Nardelli M 2003 *Phys. Rev.* B **67** 235406
[26] Damjanovic D 1998 *Rep. Prog. Phys.* **61** 1267
[27] Guy I L, Muensit S and Goldys E M 1999 *Appl. Phys. Lett.* **75** 3641
[28] Zhang Q M, Pan W Y, Jang S J and Cross L E 1988 *J. Appl. Phys.* **64** 6446
[29] Leach A R 1996 *Molecular Modelling* (London: Addison Wesley Longman Limited)
[30] Schmidt M W *et al* 1993 *J. Comput. Chem.* **14** 1347
[31] Zhang Z H, Guo W and Dai Y 2008 *Appl. Phys. Lett.* **93** 223108
[32] Baumeier B, Krüger P and Pollmann J 2007 *Phys. Rev.* B **76** 085407
[33] Zhang Z H and Guo W 2008 *Phys. Rev.* B **77** 075403
[34] Shelton D P and Rice J E 1994 *Chem. Rev.* **94** 3

Journal of Magnetism and Magnetic Materials 321 (2009) 2963–2965

Contents lists available at ScienceDirect

Journal of Magnetism and Magnetic Materials

journal homepage: www.elsevier.com/locate/jmmm

Temperature dependence of the stability of written bits in a magnetic hard-disk medium investigated by magnetic force microscopy

Yan Jiang, Wanlin Guo *

Institute of Nano Science, Nanjing University of Aeronautics and Astronautics, No. 29 Yu-Dao Street, Nanjing 210016, PR China

ARTICLE INFO

Article history:
Received 15 August 2008
Received in revised form
21 April 2009
Available online 3 May 2009

Keywords:
Thermal stability
Hard disk
Magnetic force microscope
Temperature

ABSTRACT

The thermal stability of written bits in a magnetic hard-disk medium has been investigated with a magnetic force microscope (MFM), which was equipped with an *in situ* heating system capable of heating the medium up to 300 °C. It is shown that both the annealing temperature and the duration have significant effect on the decay of the MFM signal. No signal decay is observed when annealing for 30 min up to temperatures of 200 °C. The MFM signal decays rapidly with increasing temperature, for temperatures over 200 °C. Repeated annealing at 280 °C with a duration below 10 min does not cause any signal decay.

1. Introduction

In magnetic recording, the thermal stability of recording bits and medium noise are critical factors that restrict the attainable areal density [1,2]. High areal density and signal-to-noise ratio (SNR) require a small grain size in thin-film media. However, if the magnetic grains are small enough, thermal relaxation could be caused even at room temperature and the magnetization of magnetic grains is reversed. The spontaneous magnetization reversal can result in magnetization decay and then recorded information may be lost easily [3]. To overcome this problem, high magnetic anisotropy materials are chosen. High thermal stability factor $(K_uV)/k_BT > 100$ (K_u is the uniaxial anisotropy constant of the magnetic media, V the grain volume, T the temperature in K) can be possessed by magnetic recording disks and signal decay is hardly observed at room temperature. In practice, however, the operating temperature in hard-disk drivers ranged from 60 to 150 °C or even higher and the operating duration may be up to hundreds of hours. Under such situation, the signal decay can be expected to be inevitable. Since the medium noise depends on the state of the magnetization [4], the magnetization decay can cause changes in medium noise [5], which will decrease the SNR and influence reading of the recording signal. Therefore, it is necessary to study the thermal stability of magnetic domains in hard disks at high temperature and evaluate the lifetime of the disks.

To study the thermal stability of recording media, *in situ* magnetic force microscope (MFM) observation is indispensable. Due to its very high sensitivity and resolution compared with a read head, MFM can be used to characterize qualitatively the magnetic domain structure and provide quantitative trends in the signal and SNR of recording bits as well [6–8]. In the present work, the signal decay of recording bits on a thin-film hard disk at different temperatures has been investigated by systematical MFM measurements. The signal characteristics of the hard-disk sample after being annealed are studied by analyzing the MFM images.

2. Experimental

A commercial hard disk (D540X-4K; Maxtor Co.) was used in this work. The original recording bits on the hard disk were observed at room temperature by MFM equipped with an *in situ* heating system. The sample was fixed on a special heating stage connected with a temperature controller that can be heated up to 300 °C, and the temperature was measured by a thermoelectric couple. The temperature of the magnetic film in the sample is equal to that of the heating stage. To enhance the thermal relaxation of magnetic media so that the signal decay can be observed easily, the sample was heated to 100, 150, 200, 250 and 280 °C, respectively, and sustained for 30 min at each temperature. At 280 °C, additional intermittent anneal experiments were carried out for 6 times and the sample was heated for 10 min each time. The same recording bits after annealing were observed by the MFM at room temperature. A commercial Si tip coated with magnetic films was used for MFM imaging. The tip to sample separation was 55 nm.

* Corresponding author.
E-mail address: wlguo@nuaa.edu.cn (W. Guo).

0304-8853/$ - see front matter © 2009 Elsevier B.V. All rights reserved.
doi:10.1016/j.jmmm.2009.04.063

3. Results and discussion

A series of MFM images of $1.2 \times 1.2\,\mu m^2$ area of hard disk annealed at different temperatures for 30 min are shown in Fig. 1. Well-defined rectangular bits can be observed, with the bit length of about 260 nm and the bit width of 100 nm. No significant signal decay in recording bits can be observed at the annealing temperatures below 200 °C. After a 30 min annealing at 200 °C, the edges of some recording bits become indistinct. And after annealing at 250 °C, bridging between bits is observed due to the reversal of the magnetic domains, especially along the long axis direction of the bit, and the interspaces between the upper and lower bits disappear. At the width direction of the bit, fewer bridges occur and mainly appear at the portion of the bit closest to the next one. In some bits, there are significant decays and most tend to occur at the edges. After annealing at 280 °C, the profiles of recording bits become blurry and MFM signals decay significantly. It indicates that the signal decay increases with the annealing temperature for the same sustaining duration. However, in Fig. 2, clear MFM image of bits without apparent signal decay can be seen after intermittent annealing at 280 °C for total 60 min, which shows that under a short sustaining heating duration, apparent signal decay will not occur with repeating anneal even at the temperature up to 280 °C. This suggests that the signal decay can be caused only when the annealing temperature and sustaining heating duration are high enough.

For the thermal decay of the recording signal, it has been found that the reduction of K_uV/k_BT is a major factor responsible for the serious thermal decay [9]. Each grain has one or two energy minima. The probability per unit time of magnetic grains successfully crossing the energy barrier is given by $f_0\exp(-K_uV/k_BT)$ (f_0 represents the frequency of 10^9 Hz) [10], which increases with the temperature. When the sustaining heating duration is long enough, a lot of grains may cross the energy barrier and reach the next energy minima, resulting in the reversed domain. While during the intermittent annealing, the sustaining duration in each heating cycle is not long enough for the grains to cross the energy barrier.

The written signal R_z was analyzed qualitatively by averaging the signal over some arbitrarily defined track width. R_z is defined as the average peak-to-peak value of five highest peaks and five lowest valleys. Fig. 3 shows the dependence of signal R_z of three areas outlined in Fig. 1(a) on the annealing temperature. Below 200 °C, the signal R_z appears to level off, which indicates that there is little signal decay for the sustaining duration of 30 min at the lower temperature. Above 200 °C, due to the magnetic domains reversing in the transitions, as shown in Fig. 1(e) and (f), the valleys, relative to the ones before annealing, rise up; therefore the peak-to-peak values of highest peaks and lowest valleys, corresponding to R_z, drop dramatically.

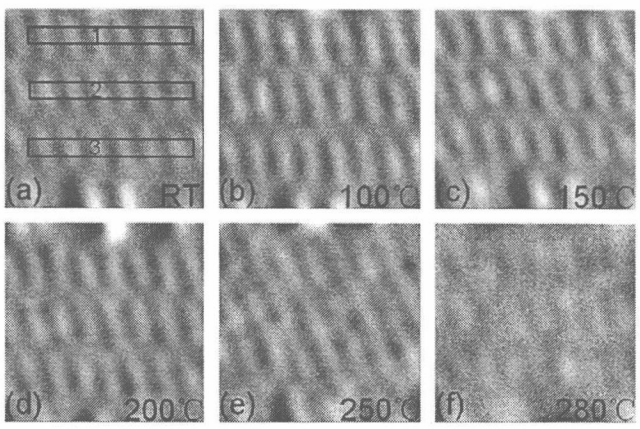

Fig. 1. MFM images of hard disk at different annealing temperatures. The size of each image is $1.2 \times 1.2\,\mu m^2$.

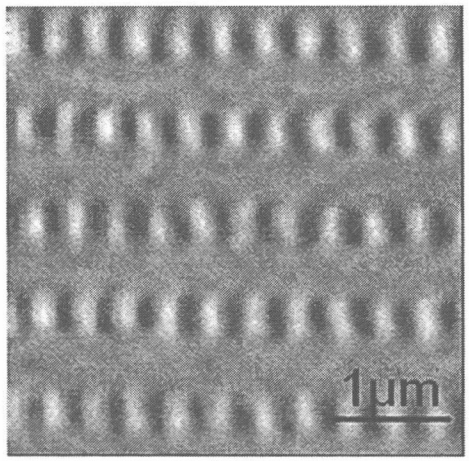

Fig. 2. MFM image of hard disk after intermittent annealing at 280 °C for 6 × 10 min.

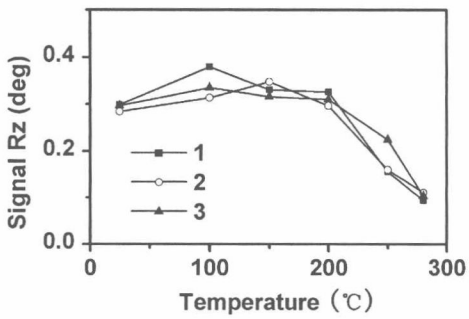

Fig. 3. Dependence of signal on the annealing temperature measured at three regions outlined by the black solid boxes in Fig. 1(a).

4. Conclusions

The signal decay due to thermal relaxation of the MFM signal of written bits in a hard disk has been studied at temperatures up to 280 °C. Measurements before and after annealing revealed that the signal decay increases with increasing annealing temperature and duration for temperatures over 200 °C. For annealing times up to 30 min, the signal remains uninfluenced up to 200 °C, but decreases dramatically with increasing annealing temperatures over 200 °C. However, repeated annealing with 10 min sustained temperatures at 280 °C causes no signal decay. Repeated annealing with constant short duration has no significant accumulation effect, at least under the tested conditions.

Acknowledgements

This work was supported by the 973 Program (No. 2007CB936204), the National NSF (No. 10372044), the Ministry of Education (No.705021, IRT0534) and Jiangsu province NSF (BK2008042) of China.

References

[1] H.J. Richter, R.M. Brockie, J.L. Pressesky, IEEE Trans. Magn. 38 (2002) 260.
[2] M. Hashimoto, K. Miura, H. Muraoka, H. Aoi, Y. Nakamura, J. Magn. Magn. Mater. 287 (2005) 123.
[3] Z. Zhang, A.K. Singh, J. Yin, A. Perumal, T. Suzuki, J. Magn. Magn. Mater. 287 (2005) 468.
[4] W. Zhu, H. Zhou, J. Judy, D. Palmer, IEEE Trans. Magn. 40 (2004) 2610.
[5] A. Taratorin, D. Cheng, E. Marinero, IEEE Trans. Magn. 36 (2000) 80.
[6] P. Arnett, T. Minvielle, S. Nair, J. Magn. Magn. Mater. 193 (1999) 479.
[7] P. Giljer, J.M. Sivertsen, J.H. Judy, C.S. Bhatia, M.F. Doerner, J. Appl. Phys. 79 (1996) 5327.
[8] K. Sin, P. Glijer, J.M. Sivertsen, J.H. Judy, IEEE Trans. Magn. 33 (1997) 1052.
[9] P.L. Lu, S.H. Charap, IEEE Trans. Magn. 30 (1994) 4230.
[10] S.H. Charap, P.L. Lu, Y. He, IEEE Trans. Magn. 33 (1997) 978.